

EVOLUTIONARY ALGORITHMS FOR THE AUTOMATIC DESIGN OF MULTIMODE MICROWAVE DIPLEXER TOPOLOGY *

Vladimir Stanovov, Sergei Khodenkov, Lev Kazakovtsev, Aleksey Popov

Reshetnev Siberian State University of Science and Technology, Russian Federation

Abstract. Computer-aided design of new microwave frequency-selective devices, including diplexers, as well as improvement of existing designs, is an important and urgent task in the field of radio engineering. The dependence of the output parameters of diplexers on their geometric parameters is complex, nonlinear, and multi-extremal. In addition, the determination of such output parameters as average frequencies and bandwidths for given geometric parameters of the microwave device design is carried out using electrodynamic modeling methods, which are very computationally expensive, and imposes restrictions on the global search algorithms used. This paper discusses algorithms for the automated synthesis of microstrip diplexer designs with adjacent passbands, implemented using dielectric monolithic substrates with both a high and low dielectric constant in calculations. Microstrip diplexers based on multimode resonators are promising microwave devices, characterized by ease of manufacture and miniature size, in which a significant improvement in the frequency-selective properties is achieved by increasing the number of resonators in them, and expanding their adjacent passbands by using resonators connected with each other electromagnetically and conductively. We investigated the possibilities of automated synthesis of these devices using special evolutionary algorithms. The efficiency of the algorithms has been shown by a computational experiment. We consider two types of devices characterized by high computational complexity of their electromagnetic modeling. The modified rate-based adaptive differential evolution algorithm is shown to be capable of finding solutions of sufficient quality with a limited resource and a specially designed objective

Received October 12, 2023. accepted November 19, 2023.

Communicated by Predrag Stanimirović

Corresponding Author: Lev Kazakovtsev, Reshetnev Siberian State University of Science and Technology, Russian Federation | E-mail: levk@bk.ru

2010 *Mathematics Subject Classification.* Primary 90C57; Secondary 90C27, 90C09

© 2023 BY UNIVERSITY OF NIŠ, SERBIA | CREATIVE COMMONS LICENSE: CC BY-NC-ND

*This work was funded by the Ministry of Science and Higher Education of the Russian Federation, State Contract FEFE-2023-0004

function. The proposed approach can be applied for automatic topology tuning of other microwave devices.

Key words: Differential Evolution; Parameter Adaptation; Electrodynamics Modeling, Microstrip Diplexer, Multimode Resonator.

1. Introduction

Nowadays, the computational intelligence (CI) technologies have found many applications in various fields of engineering. In particular, evolutionary algorithms (EAs), being a general-purpose black-box optimization tool, have become a widely applicable method in solving complex systems design problems. Some of the real world optimization problems are characterized by computationally expensive objective functions, which require modeling of physical system's properties, for example mechanical or electromagnetic ones. This requires very efficient optimization algorithms to be applied, which would not waste computational resource on unnecessary evaluations.

The domain of evolutionary algorithms today is quite vast, including various modifications of basic approaches and ideas. In numerical single-objective optimization, the leading place is often taken by the Differential Evolution (DE) algorithm [1], and its superiority is proven by many optimization competitions, organized each year [2]. The reasons for its efficiency are its simplicity, small number of parameters and well-developed methods to tune them during the algorithm run. The DE efficiently handles problems with multiple local optima, non-separability, plateaus, and different properties in different areas of the search space. There are many reports on effective DE application in various engineering problems [3].

In this study, we consider the problem of automatic design of multimode microwave diplexers. The multimode diplexers are frequency-selective microwave devices with two passbands.

Frequency-selective microwave devices are the most important elements of modern radio engineering systems. They are widely used in troposphere and satellite communication systems, as well as in various radio measuring equipment [4]. Among such devices, researchers and developers of micro-wave technology most often turn their attention to bandpass filters [5, 6], high- and low-pass filters [7, 8], and filters with two passbands [9]. In addition to the above designs, diplexers are also in demand as two-channel devices that allow frequency separation or signal combination [10]. At the same time, in terms of complexity, it is much more difficult to synthesize diplexers with given parameters than filters [11]. Therefore, the use and adaptation of search algorithms in the automated design of these microwave devices is becoming relevant and in demand.

Currently, when developing such two-channel microwave devices, special attention is paid to microstrip designs [12, 13]. They have manufacturability in production and low cost of the finished product during mass production [14]. It is also worth noting that the simulation results obtained using electrodynamic numerical analysis of their 3D models are in good agreement with the measurement results of

experimental samples [14]. This enables us to use extensively numerical experiments in exploratory studies.

Development of these promising designs implies not only a constant improvement in their electrical characteristics and a reduction in size, but also a significant expansion of the operating bandwidth which determines the width of information transmission channels. Using the design features of a microstrip conductor, we can bring together several of its lowest oscillation modes in frequencies, which enables us to form a wider bandwidth. This is an important reason to develop multi-mode devices.

Modern software for the numeric electro-dynamic analysis of microwave devices enables us to simulate the amplitude-frequency response of a microstrip device with minimal errors. Thus, such software can be used instead of physical experiments which enables us to consider a response of the device as an algorithmically described function of its geometrical parameters.

The concept of this work is to develop differential evolution algorithms for optimizing the designs of microwave microstrip diplexers including multimode ones with the use of well-known methods of electro-dynamic analysis.

Evolutionary algorithms have been previously shown to perform well for the problems of microwave devices design [11]. The microwave resonators generated with the use of DE algorithms demonstrated good frequency-selective characteristics. Moreover, the DE in combination with the electro-dynamic modelling software demonstrated the ability of exploring new perspective constructions of resonators. The constructions of the resonators generated by the DE usually coincide with the constructions designed by a qualified engineer. Diplexers are much more complex constructions, and the constructions generated automatically have sometimes surprising topology.

The DE variant used in this study is based on the well-known L-SHADE algorithm [15], which is modified with a recently proposed success rate-based scaling factor adaptation [16]. The experiments performed with two types of constructions show that the used SRDE variant is capable of finding solutions with sufficient quality using limited computational resource.

The rest of the paper is organized as follows. In Section 2, we describe general geometric configurations of the microwave diplexers to be designed. In Section 3, we state the problem mathematically and propose a differential evolution algorithm with the embedded electro-dynamical modelling. In Section 4, we describe and discuss the results of the computational experiments. In Section 5, we give a conclusion.

2. Designs of Microstrip Diplexers

2.1. Diplexers with Three Resonators

In our work, we propose and study search algorithms for the synthesis of microstrip diplexer designs implemented on monolithic dielectric substrates with high

($\varepsilon = 80$) and low dielectric constant ($\varepsilon = 9.8$). Such dielectric constants are possessed by the materials “TBNS Ceramics” and “Polikor”, which are quite common in microwave technology, respectively. The thickness of the substrates is fixed and equal to $h = 1.00$ mm. All calculations used numerical electro-dynamic analysis of 3D models of diplexers. It is assumed that a design sketch without specifying the geometric parameters is given, and the algorithm must find the geometric parameters (dimensions) of the diplexer design that best achieve the required properties of the diplexer.

The first design sketch of a microwave device is provided in Fig. 2.1, it uses a substrate with a dielectric constant of $\varepsilon = 80$.

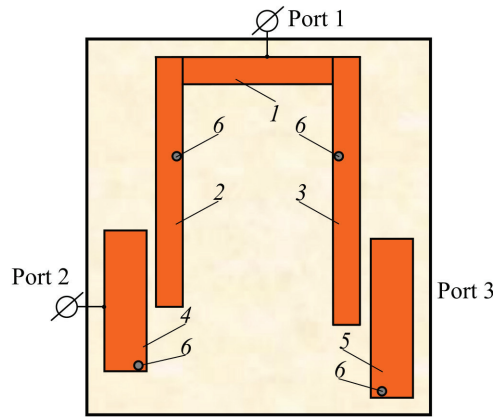


FIG. 2.1: Topology of strip conductors of a microstrip diplexer on a three-mode resonator

This microstrip diplexer uses three resonators [17]. The central three-mode resonator is formed by three sections (1-3) of strip conductor located on the substrate, grounded to the base using two identical round holes (6) filled with copper. In essence, it consists of a pair of quarter-wave resonators and one half-wave. A pair of single-mode resonators is formed by strip conductors (4) and (5) located on the substrate. Since there are also round holes (6) filled with copper at the edges of the conductors, these resonators are quarter-wave resonators.

Note that the diameter of all holes is fixed and, for definiteness, is $d \sim 0.45$ mm, and their depth is determined by the thickness of the dielectric substrate h and is equal, respectively, to 1.00 mm.

The input port of the structure (Port 1) is located on the section (1) of the central resonator, and the output ports (Port 2) and (Port 3) are located on the strip conductors (4) and (5) of the outer resonators, respectively. In this case, the conductor segment (2) is shorter than the similar segment (3), and the conductor (4) is shorter than the similar conductor (5). Their sizes are selected in such a way that the lowest resonance from each of the four quarter-wave resonators participates in the formation of two adjacent diplexer passbands. That is, a pair of such resonators

located to the left of Port 1 forms the passband of the high-frequency channel, and a pair of resonators located to the right forms the low-frequency channel, respectively. The sizes of the strip conductor sections of the central half-wave resonator are selected in such a way that its lowest resonance is located at frequencies between adjacent passbands, as shown in Fig. 2.2(b). Let us denote the frequency at which the parameters S_{21} and S_{31} in this frequency range have equal values as f_c and for definiteness, when setting up the diplexer, we will fix this parameter to $f_c = 1$ GHz.

The normalized frequency response of this diplexer is shown in Fig.2.2 in a wide (a) and narrow (b) frequency range.

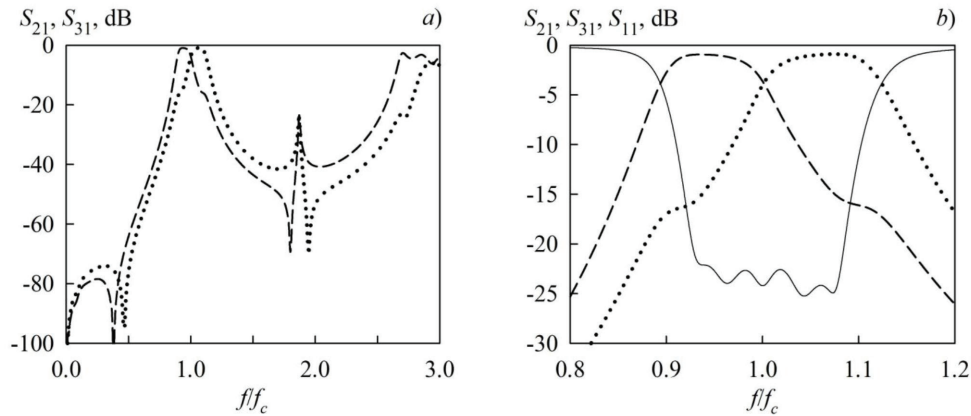


FIG. 2.2: Normalized frequency response of a microstrip diplexer based on a three-mode resonator in a wide (a) and narrow (b) frequency range

As can be seen from Fig. 2a, the considered microstrip diplexer has high-quality frequency-selective properties, and in particular, for both channels, an extended high-frequency stopband is observed on the frequency response, and strong power suppression is also observed at the frequencies of the low-frequency stopband, due to attenuation poles.

In this case, the relative bandwidth of the low-frequency channel of the diplexer, measured at a level of -3 dB from the minimum loss level $L_{1min} \approx 0.9dB$, is $\Delta f_1/f_{10} \approx 11.3\%$. For the passband of a high-frequency channel, this value is $\Delta f_2/f_{20} \approx 11.5\%$, while the level of minimum losses is similar, $L_{2min} \approx 0.9dB$.

To implement a diplexer with significantly expanded adjacent passbands, let us consider the design presented in Fig. 2.3. The development and research of such devices is a relevant and important direction in modern microwave technology, because this enables us to increase the data transfer speed in wireless networks.

This microstrip diplexer also uses three resonators. The central resonator consists of interconnected strip sections (7)-(11) located on a dielectric substrate. The input signal arrives at Port 1, located on a wide segment (9), on the side opposite the free end. A pair of outer resonators is formed by strip sections (1)-(5) and (13)-

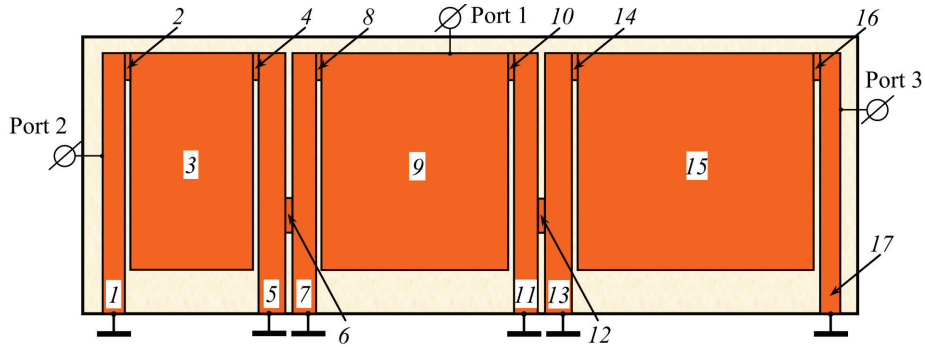


FIG. 2.3: Topology of microstrip conductors of a three-resonator diplexer

(17), respectively. The transmitted signal arrives at Port 2, located on an extended section (1) of the resonator located to the left of the central one. Similarly, the transmitted signal also arrives at Port 3, located on an extended section (17) of the resonator located to the right of the central one. Since each pair of extreme segments of all three resonators is connected at one end to a grounded base, the resonators used in the design are half-wave.

Due to the fact that the wide segment (3) of the outermost resonator, located to the left of the central one, has the smallest width compared to similar segments (9) and (15) of the other two resonators, its lowest resonance participates in the formation of the high-frequency passband of the diplexer (Fig. 2.4, part b). At the same time, the wide segment (15) of the outermost resonator, located to the right of the central one, on the contrary, has the greatest width compared to similar segments (3) and (9) of the other two resonators, therefore its lowest resonance participates in the formation of low-frequency diplexer bandwidth. Finally, the wide section (9) of the central resonator has a width greater than that of a similar section (3) of the resonator located to the left of it, but smaller than that of a similar section (15) of the resonator located to the right of it, therefore, its the lowest resonance is at frequencies between adjacent passbands.

Adjacent sections (5) and (7) of the outer and central resonators, grounded to the base at one end, are connected to each other through a jumper section (6). Similarly, adjacent sections (11) and (13) of the central and outer resonators are connected to each other through a jumper section (12). Thus, the resonators in the diplexer are connected to each other electromagnetically and additionally conductively due to such jumper segments. It is important to note that by changing the length and width of the jumper sections, as well as their vertical displacement, you can significantly expand the bandwidth of each diplexer channel.

When synthesizing this diplexer, a substrate with a lower dielectric constant $\varepsilon = 9.8$ was used, so, the f_c value was chosen equal to 3 GHz. The normalized frequency response of this design is shown in Fig.2.4 in a wide (a) and narrow (b) frequency range.

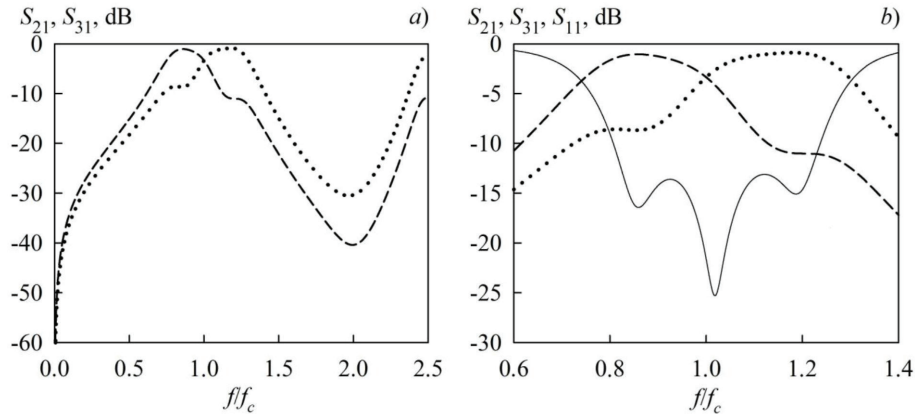


FIG. 2.4: Normalized frequency response of a microstrip three-mode diplexer in a wide (a) and narrow (b) frequency range

Table 2.1: Dimensions of strip conductor sections of three-resonator diplexers, Fig. 2.1

Position of the strip conductor section	Strip cut dimensions conductor, mm ²
(1)	8.65×1.50
(2)	14.40×1.50
(3)	15.35×1.50
(4)	8.10×2.40
(5)	9.15×2.40

It can be seen from the figure that the high-frequency stopband of each diplexer channel is significantly expanded, which is explained by a large jump in the wave impedances of the microstrip line segments. The relative bandwidth of the low-frequency channel of the diplexer, measured at a level of -3 dB from the level of minimum losses $L_{1min} \approx 1.0$ dB, is $\Delta f_1/f_{10} \approx 30\%$, and for the high-frequency channel, it is $\Delta f_2/f_{20} \approx 26\%$ at $L_{2min} \approx 0.9$ dB, respectively. It is important to note that the relative bandwidth of this design is more than twice as wide as that of the previous one.

The dimensions of the strip conductor sections of the synthesized diplexers shown in Fig. 2.1 and Fig. 2.3 are given in Tables 2.1 and 2.2 as an example.

Note that for the design shown in Fig. 2.1, the displacement of the centers of the round through holes (6) in the central strip conductor relative to its upper edge is 5.75 mm. The displacement of the lower edge of the strip conductor (4) relative to the lower edge of the strip conductor segment (2) is 3.60 mm, and the displacement of the lower edge of the strip conductor (5) relative to the lower edge of the strip conductor segment (3) is 4.10 mm. The dimensions of the pair of gaps between the strip conductors and the conductor sections are the same and amount to 0.60 mm

Table 2.2: Dimensions of strip conductor sections of three-resonator diplexers, Fig. 2.3

Position of the strip conductor section	Strip cut dimensions conductor, mm ²
(1)	6.05×0.55
(2)	0.60×0.10
(3)	5.05×2.90
(4)	0.60×0.10
(5)	6.05×0.65
(6)	0.85×0.15
(7)	6.05×0.60
(8)	0.60×0.10
(9)	5.05×4.45
(10)	0.60×0.10
(11)	6.05×0.60
(12)	0.85×0.15
(13)	6.05×0.65
(14)	0.60×0.10
(15)	5.60×5.05
(16)	0.60×0.10
(17)	6.05×0.55

(between (5) and (3) and between (4) and (2)). The area of the monolithic bed of this diplexer was 18.65×21.45 mm².

For the design shown in Fig. 2.3, the displacement of segments (6) and (12) from the edge of the support on the side of the connection of the segments to the grounded base is 1.85 mm. The displacement of Port 2 and Port 3 from the edge of the support on the side of the connection of the segments to the grounded base is 3.65 mm, 4.75 mm, respectively. The offset of Port 1 from the left edge of the segment (9) is 3.75 mm. The area of the monolithic bed of this diplexer was 7.05×19.45 mm².

2.2. Five-Resonator Microstrip Diplexers

Improving the frequency-selective properties of the microstrip diplexer presented in Fig. 2.3 can be achieved by increasing the number of resonators located on both sides of its central resonator. In this case, one resonance can be added from each of such resonators to one of the adjacent passbands of the diplexer. The five-resonator microwave diplexer constructed in this way is shown in Fig.2.5. For the convenience of comparing the characteristics of the structures with each other, a dielectric substrate with similar parameters was used in the calculations - its dielectric constant $\varepsilon = 9.8$, and thickness $h = 1.00$ mm. When configuring the microstrip diplexer, the f_c value was also fixed and also equal to 3 GHz.

Its amplitude-frequency characteristics, as well as the frequency response of the diplexers discussed above, are shown in a wide and narrow frequency range in the

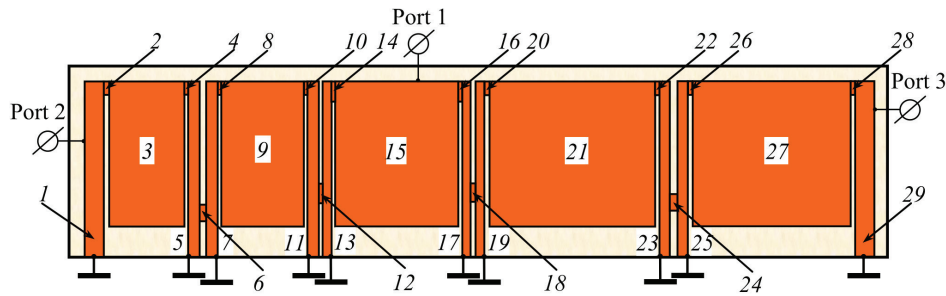


FIG. 2.5: Topology of microstrip conductors of a five-resonator diplexer

Fig. 2.6.

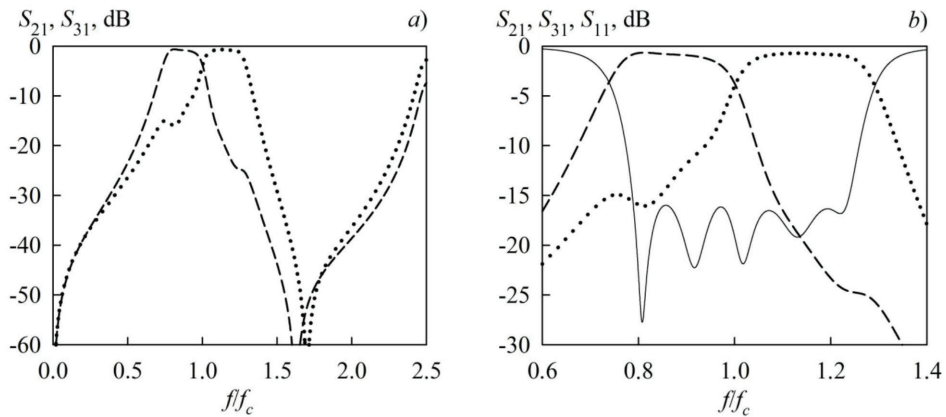


FIG. 2.6: Normalized frequency response of a microstrip five-resonator diplexer in a wide (a) and narrow (b) frequency range

Note that, in comparison with a similar three-resonator diplexer (see Fig. 2.3 and Fig. 2.4), this design has a significant increase in the slope of the passbands of both channels, an increase in power suppression at frequencies of both low-frequency and high-frequency stop bands, as well as more uniform power flow at frequencies of adjacent passbands.

In this case, the relative bandwidth of the low-frequency channel of the diplexer, measured at a level of -3 dB from the minimum loss level $L_{1min} \approx 0.7$ dB, is $\Delta f_1/f_{10} \approx 30\%$. For the passband of a high-frequency channel, this value is $\Delta f_2/f_{20} \approx 25\%$, while the level of minimum losses is similar, $L_{2min} \approx 0.7$ dB.

The dimensions of the strip conductor sections of this diplexer, similarly as for the designs discussed above, are given in Table 2.3.

Table 2.3: Dimensions of strip conductor sections of three-resonator diplexers, Fig. 2.5

Position of the strip conductor section	Strip cut dimensions conductor, mm ²
(1)	5.90×0.70
(2)	0.50×0.10
(3)	4.90×2.55
(4)	0.50×0.10
(5)	5.90×0.40
(6)	0.55×0.20
(7)	5.90×0.40
(8)	0.50×0.10
(9)	4.90×2.85
(10)	0.50×0.10
(11)	5.90×0.35
(12)	0.65×0.15
(13)	5.90×0.30
(14)	0.70×0.10
(15)	4.90×4.15
(16)	0.70×0.10
(17)	5.90×0.30
(18)	0.65×0.15
(19)	5.90×0.35
(20)	0.50×0.10
(21)	5.60×4.90
(22)	0.50×0.10
(23)	5.90×0.40
(24)	0.55×0.20
(25)	5.90×0.40
(26)	0.50×0.10
(27)	5.35×4.85
(28)	0.50×0.10
(29)	5.90×0.70

The displacement of the sections of strip conductors (6), (12), (18), (24) from the edge of the support on the side of the connection of the sections to the grounded base was 1.20 mm, 1.80 mm, 1.85 mm, 1.55 mm, respectively. The displacement of Port 2 and Port 3 from the edge of the support on the side of the connection of the segments to the grounded base is 3.90 mm, 5.00 mm, respectively. The offset of Port 1 from the left edge of the segment (15) is 3.20 mm. The area of the monolithic bed of this diplexer was 6.90×28.50 mm².

3. Proposed approach

In order to perform a search for optimal topology of diplexers, two main parts are required. First of all, the problem should be mathematically formulated, i.e. the requirements to the frequency characteristics should be described as functions. Secondly, the suitable optimization method should be chosen to solve the formulated problem. In the next subsection, we formulated objective function.

3.1. Objective function

The constrained optimization problems can be solved using various approaches, one of which is to apply a weighted sum of objectives and constraints. The development of the solutions evaluation method is one of the most complicated part, as it should consider all the requirements for the multimode diplexers. In this study, the fitness function was constructed as follows:

$$Fit(S) = f_{11}(S) + f_{21}(S) + f_{31}(S) + 50 \cdot g_1(S) + 50 \cdot g_2(S) + g_3(S) + g_4(S) + g_5(S), \quad (3.1)$$

$$f_{11}(S) = \frac{\sum_{i=lf_i}^{hf_i} \begin{cases} e^{S_{11}(i) \cdot 0.25} & \text{if } S_{11}(i) > -TH \\ e^{S_{11}(i) \cdot 0.05} & \text{otherwise} \end{cases}}{hf_i - lf_i} \quad (3.2)$$

$$f_{21}(S) = \frac{\sum_{i=lf_i}^{mf_i} e^{-S_{21}(i) \cdot 0.25}}{mf_i - lf_i} + \frac{\sum_{i=1}^{lf_i} e^{(-S_{21}(i)+3) \cdot 0.05} + \sum_{i=mf_i}^n e^{(-S_{21}(i)+3) \cdot 0.05}}{lf_i + n - mf_i} \quad (3.3)$$

$$f_{31}(S) = \frac{\sum_{i=mf_i}^{hf_i} e^{-S_{31}(i) \cdot 0.25}}{hf_i - mf_i} + \frac{\sum_{i=1}^{mf_i} e^{(-S_{31}(i)+3) \cdot 0.05} + \sum_{i=hf_i}^n e^{(-S_{31}(i)+3) \cdot 0.05}}{lf_i + n - mf_i} \quad (3.4)$$

$$g_1(S) = \left| \frac{S_{21}(mf_b) + S_{21}(lf_b)}{2} - \frac{mf_i - lf_i}{2} \right| + \left| \frac{2(S_{21}(mf_b) - S_{21}(lf_b))}{S_{21}(mf_b) + S_{21}(lf_b)} - \frac{2(mf_i - lf_i)}{mf_i + lf_i} \right|, \quad (3.5)$$

$$g_2(S) = \left| \frac{S_{31}(hfb) + S_{31}(mfb)}{2} - \frac{hfi - mfi}{2} \right| + \left| \frac{2(S_{31}(hfb) - S_{31}(mfb))}{S_{31}(hfb) + S_{31}(mfb)} - \frac{2(hfi - mfi)}{hfi + mfi} \right|, \quad (3.6)$$

$$g_3(S) = \begin{cases} 10 \left(\max_{i \in \{lfb, hfb\}} S_{11}(i) + TH \right), & \text{if } \max_{i \in \{lfb, hfb\}} S_{11}(i) > -TH \\ 0, & \text{otherwise} \end{cases}, \quad (3.7)$$

$$g_4(S) = 50 |nmod(S_{11}) - nmod_g| \quad (3.8)$$

$$g_5(S) = \begin{cases} 50, & \text{if } \frac{S_{21}(mfb) + S_{21}(lfb)}{2} > \frac{S_{31}(hfb) + S_{31}(mfb)}{2}, \\ 0, & \text{otherwise.} \end{cases}, \quad (3.9)$$

Here, $TH = 14$ is the threshold indicating that losses exceeding $-14dB$ in reflection should be eliminated, lfi , mfi and hfi are the desired lower, middle and higher frequency parameters, which are indexes in the S -values array, n is the total number of S measurements, lfb , mfb and hfb are the measured indexes, determined at the $-3dB$ level, $nmod$ and $nmod_t$ are the measured and target number of modes. Thus, the fitness function combines several methods of measuring the solution quality. First, the exponential curves are used to keep the S -parameters from falling into undesired regions, and both frequency and dB levels are considered. Second, the average frequencies and desired averages are compared for each channel. Finally, the number of modes, as well as positions of the channels are considered.

In particular, $f_{11}(S)$ works as follows. If the S_{11} value within the region from lfi to hfi is above the threshold $TH = 14$, then the values increase exponentially with a large parameter of 0.25, while for values below TH the penalty is very small. Functions $f_{21}(S)$ and $f_{31}(S)$ are similar in a sense that they implement the same procedure for evaluating the curves for first and second channel. In particular, within the range from mfi to lfi , the values of S_{21} should be close to zero, while outside they should be negative. The graphical representation of these three functions is shown in Fig. 3.1, where brighter color shows higher penalty for the curve for reaching this region.

Function $g_1(S)$ evaluates the distance between the desired and actual position of the mean for S_{21} in the first part, while the second part is responsible for the width of the curve within lfi to mfi range. The same is true for function $g_2(S)$, which evaluates the quality of S_{31} in range mfi to hfi . The $g_3(S)$ is non-zero if the S_{11} curve exceeds the threshold, and is zero otherwise. The $g_4(S)$ is non-zero if the number of desired modes is different from the actual one. Finally, $g_5(S)$ is needed to make sure that the peak of S_{21} is on the left of S_{31} , and if this is not true, a penalty is applied.

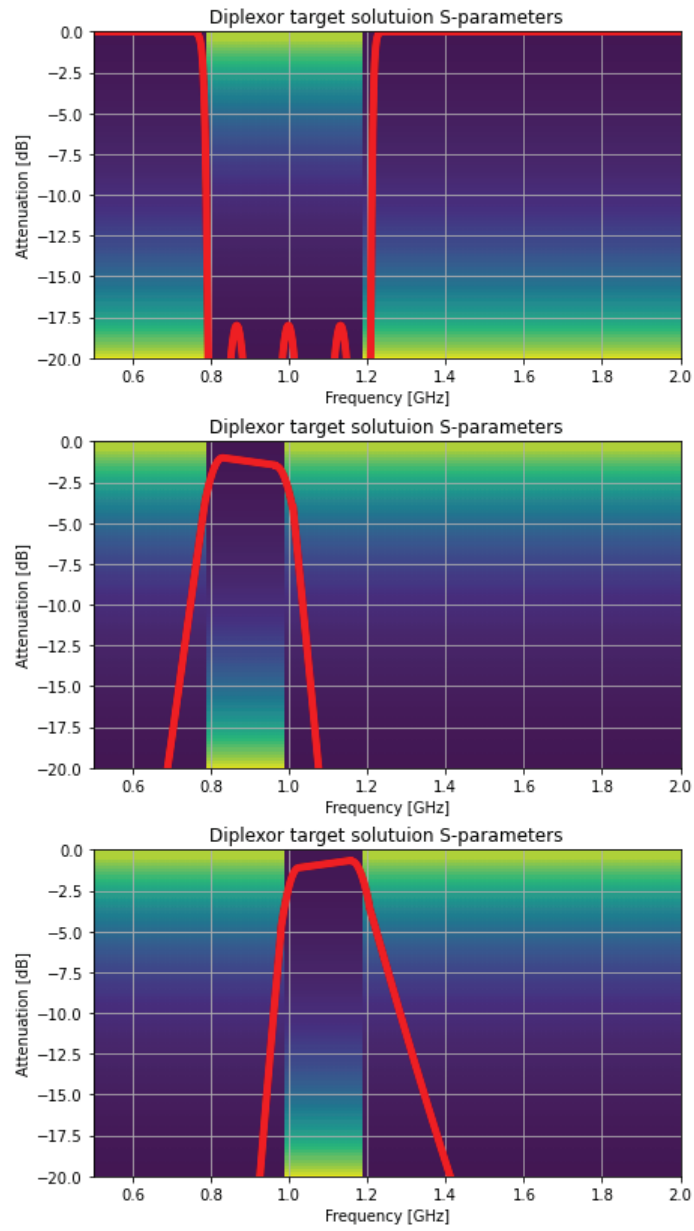


FIG. 3.1: An example of the diplexer evaluation criteria

3.2. Optimization algorithm

The formulated optimization problem has numeric variables, and can be classified as a black-box problem, as derivatives are not available, and the structure of the search

space is not known beforehand. There are many zero order numerical optimization methods available in the literature, but the computational complexity of the diplexer design requires highly efficient optimizer to be used, as long simulation time limits the number of objective (fitness) function available in the reasonable time. In this study a variant of the differential evolution [18] algorithm was used, in particular, the modification of the success-history based adaptive DE (SHADE) [19].

The differential evolution algorithm starts by initializing a set (population) of solutions in a D -dimensional search space using some random sampling method. If the search space boundaries are well known, the uniform distribution of points in the search space is applied. However, in this study the normal distribution was used, and the seed solution coordinates were used as mean values. In particular, the initialization of a population with N individuals was performed as follows:

$$x_{i,j} \sim \mathcal{N}(xs_j, 0.2 \cdot xs_j). \quad (3.10)$$

Here, xs_j is the j -th coordinate of the seed solution xs , $\mathcal{N}(\mu, \sigma)$ is a normally distributed random number with mean μ and standard deviation σ , $x_{i,j}$ is the j -th coordinate of the i -th individual, $i = 1, 2, \dots, N$, $j = 1, 2, \dots, D$. The standard deviations are set as 20% of the initial values of the parameters. After determining the positions of individuals, the fitness values $fit(x_i)$ are calculated using the objective function.

After the population is initialized, the mutation step is performed. The well-known *current-to-pbest* mutation strategy, proposed in JADE [20] is applied to generate mutant vector:

$$v_{i,j} = x_{i,j} + F(x_{pb,j} - x_{i,j}) + F(x_{r1,j} - x_{r2,j}). \quad (3.11)$$

Here, v_i is the mutant vector, F is the scaling factor parameter, pb is the index of one of the $p\%$ best individuals, $r1$ is an index, randomly chosen with selective pressure, and $r2$ is chosen using uniform random distribution from either current population x or external archive xa . The external archive is formed from replaced parent individuals during selection step.

The $r1$ index is determined using discrete distribution, which is derived from the ranking of individuals and their corresponding fitness values. For this purpose the fitness values $fit(x_i)$ of individuals are sorted, and individuals are assigned ranks r_i , based on which the probabilities are calculated:

$$p_i = e^{\frac{-i}{sp \cdot N}}, \quad (3.12)$$

where $sp = 3$ is the selective pressure parameter. The probabilities are then assigned to individuals, and a discrete distribution is applied to determine $r1$ index. The selective pressure, considered in [21] and [22], allows faster convergence and more directed search process.

The pb value is set based on the ranking of individuals by fitness, in particular, the p parameter was set to 0.3, i.e. one of the 30% best individuals is chosen.

The setting of the F parameter, scaling factor, is one of the most difficult parts of any DE-based algorithm, as this parameter has high sensitivity. In this study we used the success rate-based adaptation instead of a more classical success history-based adaptation. For this purpose the success rate SR , determined during selection step, is used to sample F values using Cauchy distribution:

$$F = randc(SR^{\frac{1}{4}}, 0.1). \quad (3.13)$$

Here, $randc(m, s)$ is a Cauchy-distributed random value with location parameter m and scale parameter s . If the generated F is negative, it is sampled again until positive, and if $F > 1$, then it is set to $F = 1$. If the success rate is high, it will result in larger F values, thus moving towards one of the pb solutions, i.e. more exploitation, but if the success rate is low, so will be the F values, i.e. more exploration of the search space will occur. Similar approach was considered in [23].

After mutation step, the crossover is performed between the mutant vector v_i and target vector x_i . The widely used binomial crossover is used in this study:

$$u_{i,j} = \begin{cases} v_{i,j}, & \text{if } rand(0, 1) < Cr \text{ or } j = jrand, \\ x_{i,j} & \text{otherwise.} \end{cases} \quad (3.14)$$

Here, u_i is the trial vector, $rand(0, 1)$ is a uniformly distributed random value in range $[0, 1]$, Cr is the crossover rate parameter, and $jrand = rand(1, D)$ is a random integer value, which is set to one of the coordinates indexes to make sure that at least one of the coordinates is inherited from the trial vector. Otherwise u_i can be the same as x_i , which would lead to pointless objective function evaluation.

The Cr parameter in this study is determined using normal distribution as follows:

$$Cr \sim \mathcal{N}(0.9, 0.1). \quad (3.15)$$

If the sampled Cr value was smaller than 0 or larger than 1, it was clipped to $[0, 1]$ interval.

The next step of DE is the selection, where the newly generated trial vector is compared to the target vector using fitness values.

$$x_{i,j} = \begin{cases} u_{i,j}, & \text{if } fit(u_i) < fit(x_i) \\ x_{i,j} & \text{otherwise} \end{cases} \quad (3.16)$$

In other words, if the newly generated solution is better than the current individual on the i -th position, then the replacement occurs, and the fitness value is updated as well. The replaced parent solution x_i is then copied into the external archive xs . Initially the archive is filled with randomly sampled individuals, and random indexes are used for replacement.

The number of successful replacements determines the success rate:

$$SR = \frac{S}{N} \quad (3.17)$$

where S is the number of times when $fit(u_i)$ was smaller than $fit(x_i)$.

The described algorithm will be further referred to as SRDE (Success Rate-based Differential Evolution).

3.3. Optimized constructions

The first diplexer construction considered in this study and the scattering parameters of the presented topology are shown in Fig. 3.2. This is a seed solution, i.e. the one from which all optimization started.

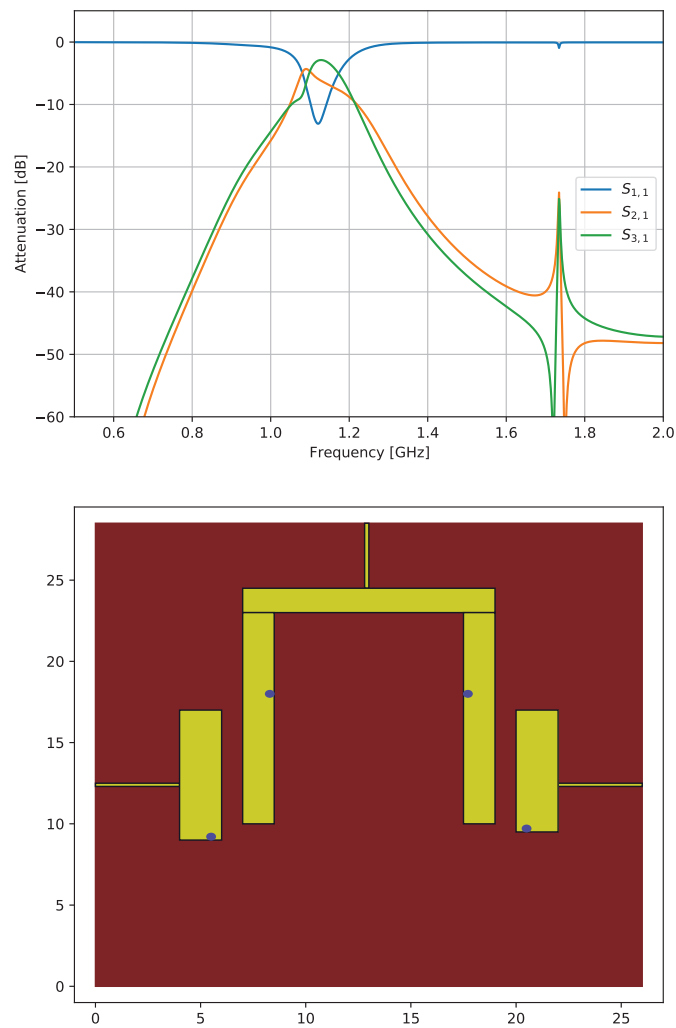


FIG. 3.2: Diplexer seed solution S-parameters and topology, first construction

As can be seen from Fig. 3.2, the construction is simmetrical, which does not make it a diplexer yet. The blue circles are the grounding copper columns. The substrate is the TBNS with $\varepsilon = 80$ and $\mu = 1$. The thickness of the substrate is $0.98mm$, and the copper layer is $0.02mm$ thick. The port connectors are $4mm$ long and $0.2mm$ wide, grounding cylinders have $0.2mm$ radius. The optimization algorithm is allowed to change the shapes of all rectangles, as well as their positions and positions of cylinder grounding, which makes a total of 26 variables to be optimized. The characteristics of the seed solution are far from a proper diplexer shown in Fig 3.2. Fig. 3.3 shows the desired characteristics.

As shown in Fig. 3.3, the desired solution has two separate channels, from 0.8 to 1.0GHz and from 1.0 to 1.2GHz. The goal of the optimization algorithm is, therefore, to perform the search for the solution, that would be as close to the desired one as possible.

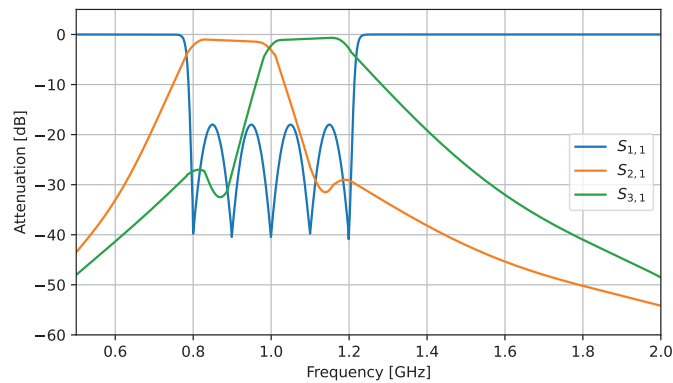


FIG. 3.3: Diplexer target solution S-parameters, the first construction

4. Results and Discussion

The computational experiments included running the optimization algorithm SRDE several times and recording all the considered topologies of multimode diplexers. There were 4 independent runs performed, and the population size N was set equal to $D = 26$ variables. The algorithm ran for 2000 target function evaluations (simulations), each taking around 5-7 minutes on an Intel Core i7 13700KF processor, the source code was written in Python 3.8.

Fig 4.1-4.4 show the S-parameters of the obtained solutions and corresponding topologies.

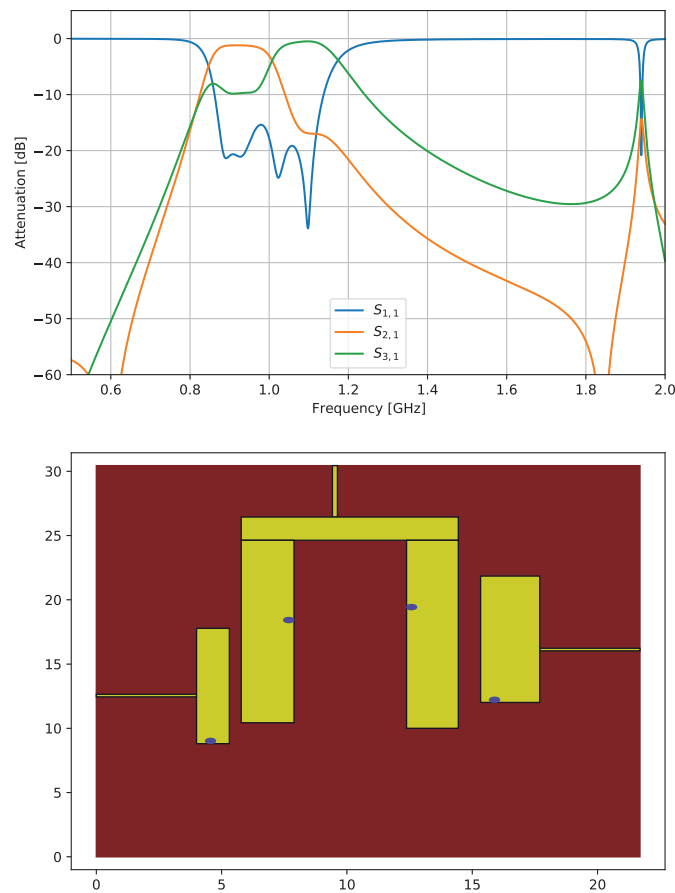


FIG. 4.1: Obtained solution S-parameters and topology, the first run, first the construction

As can be seen from Fig. 4.1-4.4, the found solutions are quite diverse, i.e. the topologies differ very much, although all of them are quite close to the desired solution characteristics. The solution from the third run has four modes, however, it is highly assymetrical and have certain problems with $S_{3,1}$ AFC curve.

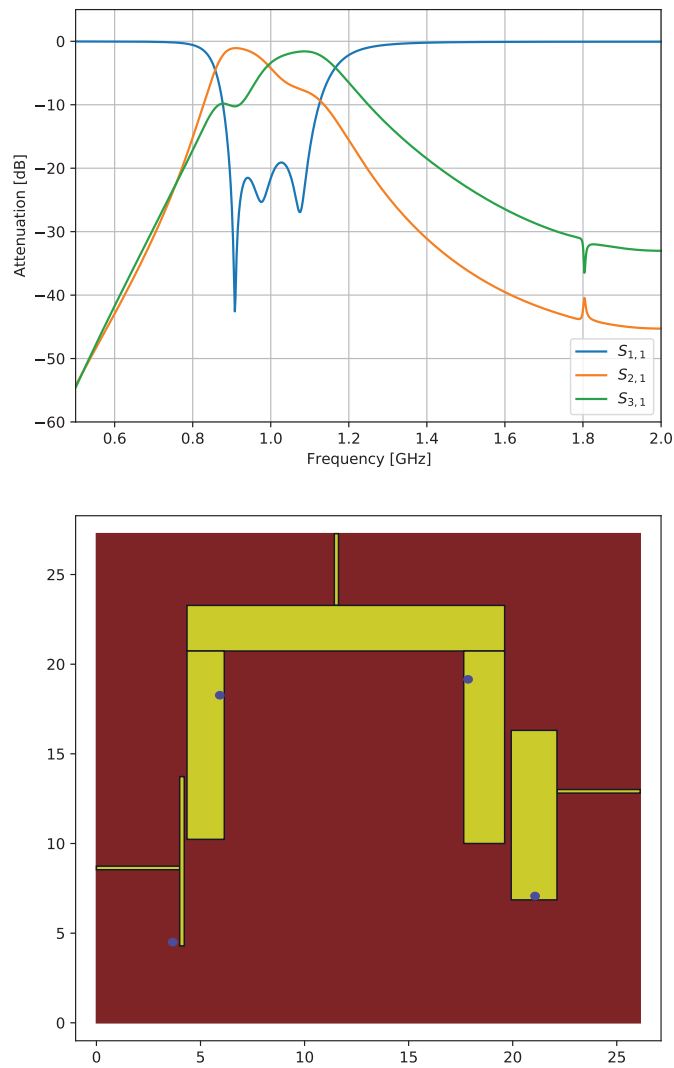


FIG. 4.2: Obtained solution S-parameters and topology, the second run, the first construction

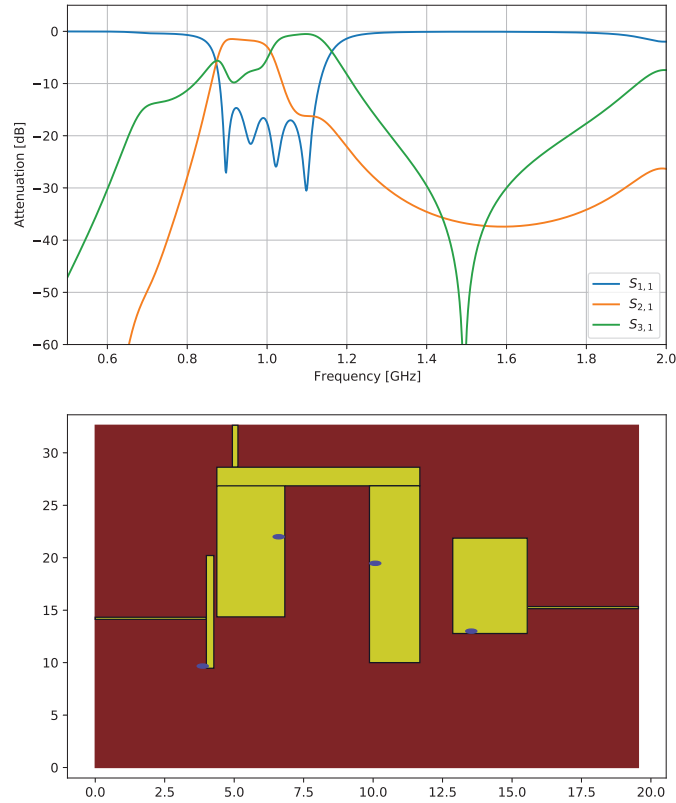


FIG. 4.3: Obtained solution S-parameters and topology, the third run, the first construction

To demonstrate the convergence process, in Fig. 4.5, all fitness values, which were recorded during fourth run, are shown.

Fig. 4.5 demonstrates that during the first 300-500 evaluations the initial fast convergence occurs, and next a slower search process begins. By around 1500 fitness evaluations the curve oscillations almost flatten, and only small improvements to the best solution are made. Nevertheless, the best solutions throughout the whole search are always found at one of the last generations. Such fitness graph means that the population size is relatively small for a problem of this level of complexity, however, larger population size would result in a longer convergence, and 2000 evaluations may not be enough to get a solution of a desired quality.

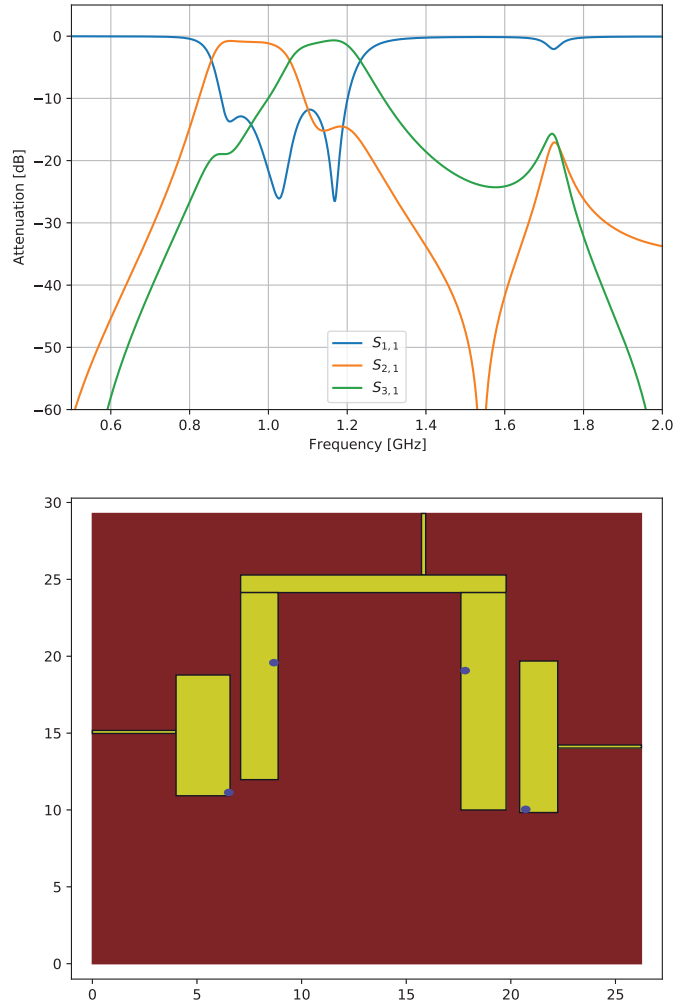


FIG. 4.4: Obtained solution S-parameters and topology, fourth run, first construction

For the second construction, the seed solution is shown in Fig. 4.6.

As can be seen from Fig. 4.6, the initial seed solution is a symmetrical construction, which does not function as a diplexer. The goal of the optimization here is again to tune the topology to meet the requirements. Here the desired goal frequencies are from 2.4 to 3.25GHz and from 3.25 to 4.1GHz.

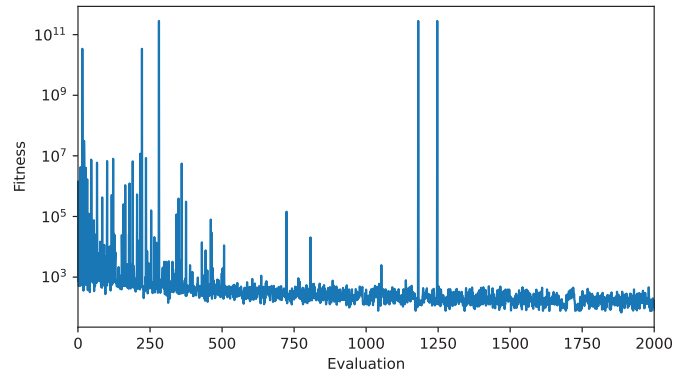


FIG. 4.5: Fitness values, fourth run

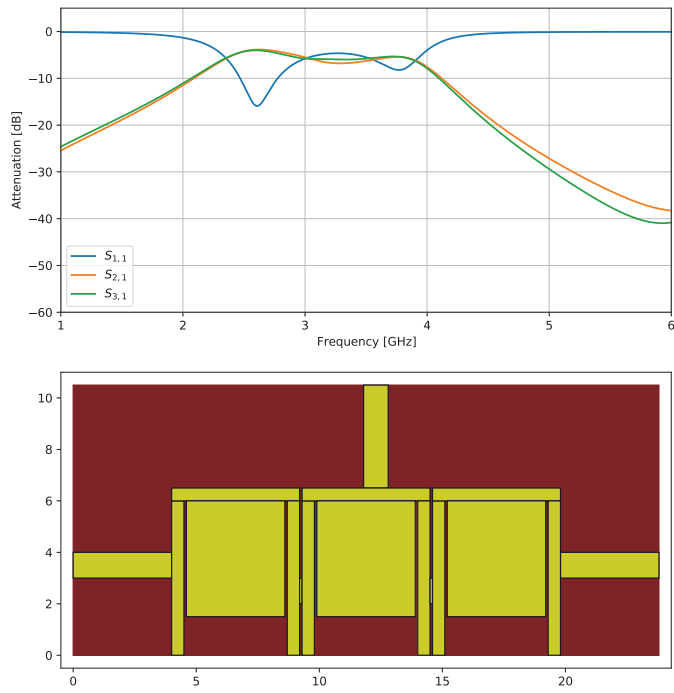


FIG. 4.6: Diplexer seed solution S-parameters and topology, second construction

Figures 4.7-4.10 show the S-parameters of the obtained solutions and corresponding topologies.

Considering the found topologies, shown in Fig. 4.7-4.10, one may see that in all cases the DE algorithm has decided to make the central part higher compared to the side ones. That is, the tuning is mainly done by height adjustment, and not by width adjustment, which is a typical approach taken by specialists, who do the tuning by hand. It shows that the algorithm has taken a different route in solving the problem, probably an easier one. Such information can be further used by experts in the field.

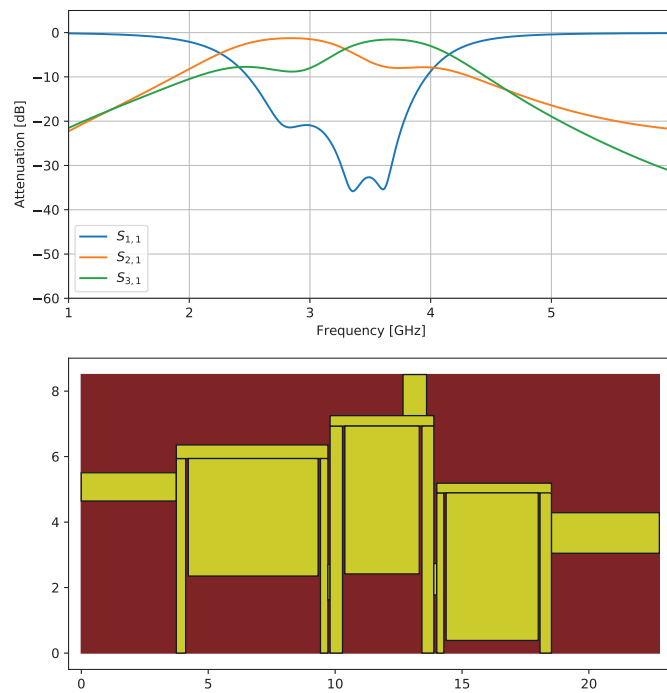


FIG. 4.7: Obtained solution S-parameters and topology, first run, second construction

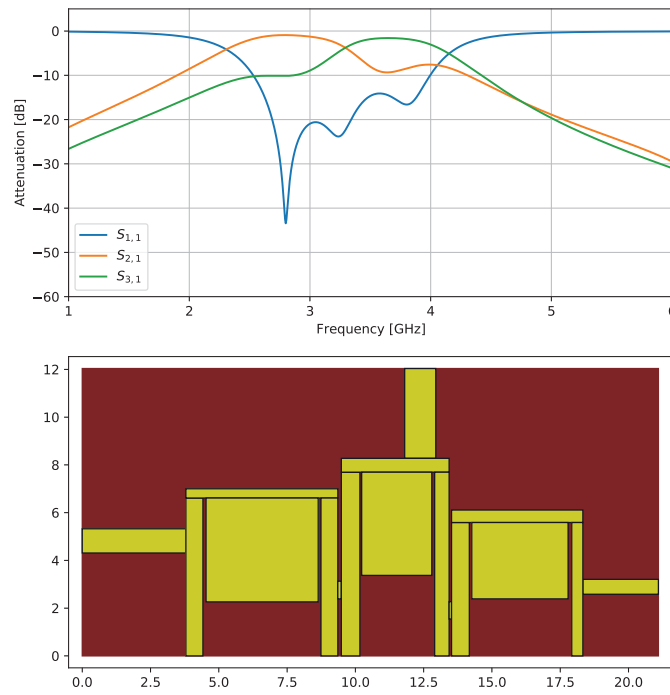


FIG. 4.8: Obtained solution S-parameters and topology, second run, second construction

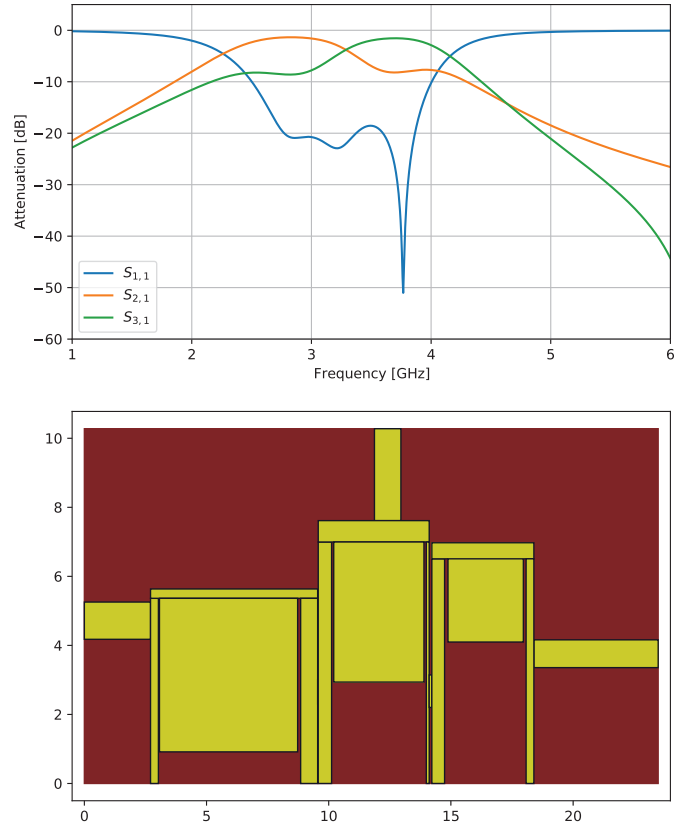


FIG. 4.9: Obtained solution S-parameters and topology, third run, second construction

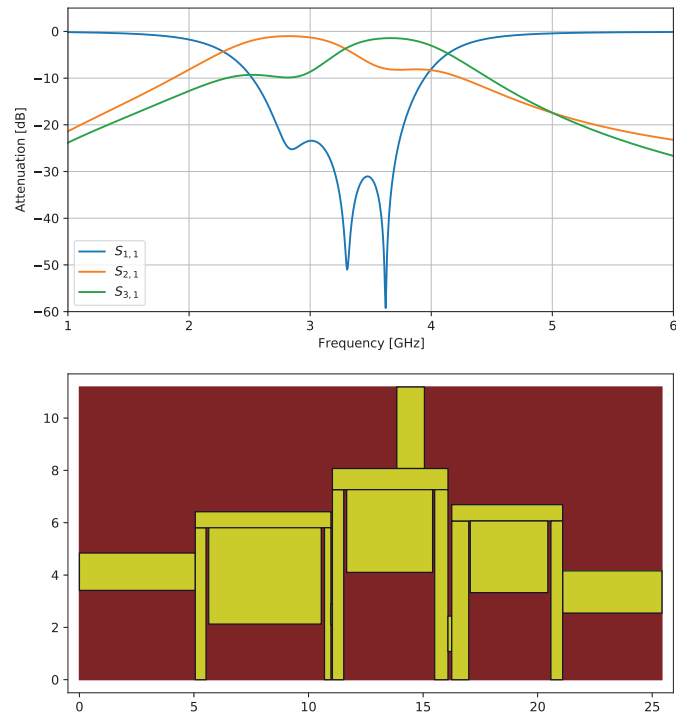


FIG. 4.10: Obtained solution S-parameters and topology, fourth run, second construction

5. Conclusion

This study has shown that the complex topology optimization problems can be efficiently solved by the differential evolution algorithm SRDE despite the large number of variables to be tuned and a very limited computational resource. Applying the same approach for two different problems shows that it can be efficiently used for similar problems, i.e. it shows the universality of the algorithm. Further studies in this direction may include experiments with even more complex topologies and simplification of the target function.

The automated design of the microwave resonators [11] usually results in the same constructions as a qualified engineer develops after approximately 2-4 weeks of work. For diplexers, the automatically generated constructions are surprising for the engineers, and the proposed algorithm not only improves the efficiency of the engineer's work, but also enables us to develop new constructions with unexpected geometry.

REFERENCES

1. S. DAS and P.N. SUGANTHAN: *Differential evolution: a survey of the state-of-the-art*. IEEE Transactions on Evolutionary Computation. **15** (1) (2011), 4-31. <https://doi.org/10.1109/TEVC.2010.2059031>.
2. A. P. PIOTROWSKI and J. J. NAPIORKOWSKI: *Step-by-step improvement of JADE and SHADE-based algorithms: Success or failure?*. Swarm and Evolutionary Computation. **43** (2018), 88-108, doi = <https://doi.org/10.1016/j.swevo.2018.03.007>.
3. S. DAS and S.S. MULLICK AND P.N. SUGANTHAN: *Recent advances in differential evolution – an updated survey*. Swarm and Evolutionary Computation. **27** (2016), 1-30, <https://doi.org/10.1016/j.swevo.2016.01.004>.
4. J.-S. HONG: *Microstrip filters for RF/microwave applications*. Hoboken: John Wiley & Sons, Inc. (2011).
5. M.-H. HO and W.-C. LIN: *Design of stepped-impedance hairpins band-pass filter with wide stopband performance*. Microwave and Optical Technology Letters. **52**(6) (2010), 1405-1408.
6. K.-W. HSU and W.-H. TU: *Design of compact microstrip band-pass filter with ultra-wide stopband*. Microwave and Optical Technology. **52**(7) (2010), 1603-1606.
7. Z. HAO and J. HONG: *UWB Bandpass Filter Using Cascaded Miniature High-Pass and Low-Pass Filters with Multilayer Liquid Crystal Polymer Technology*. IEEE Transactions on Microwave Theory and Techniques. **58**(4) (2010), 941-948.
8. B.A. BELYAEV, S.A. KHODENKOV, R.G. GALEEV and V.F. SHABANOV: *A Low-pass Filter Based on a 2D Microstrip Electromagnetic Crystal*. Doklady Physics. **63** (2019), 85–89.
9. K. SONG, F. ZHANG, CH. ZHUGE and Y. FAN: *Compact Dual-band Bandpass Filter Using Spiral Resonators and Short-circuited Stub-loaded Resonator*. Microwave and Optical Technology Letters. **55**(06) (2013), 1393-1398.

10. H.-S. PENG and Y.-C. CHIANG: *Microstrip Diplexer Constructed with New Types of DualMode Ring Filters*. IEEE Microwave and Wireless Components Letters. **25(1)** (2015), 7-9.
11. V. V. STANOVOV, S. A. KHODENKOV, A. M. POPOV and L. A. KAZAKOVTSEV: *The Automatic Design of Multimode Resonator Topology with Evolutionary Algorithms*. Sensors. **22** (2022), <https://api.semanticscholar.org/CorpusID:247242349>
12. J. K. XIAO, M. ZHU, Y. LI, L. TIAN and J. G. MA: *High Selective Microstrip Bandpass Filter and Diplexer with Mixed Electromagnetic Coupling*. IEEE Microwave and Wireless Components Letters. **25(12)** (2015), 781-783.
13. Y. S. MEZAAL, S. A. HASHIM, A. H. ALFATLAWI and H. A. HUSSEIN: *New Microstrip Diplexer for Recent Wireless Applications*. International Journal of Engineering and Technology. **7** (2018), 96-99.
14. B. A. BELYAEV, A. M. SERZHANTOV and V. V. TYURNEV: *A Dual-Mode Split Microstrip Resonator and Its Application in Frequency Selective Devices*. Microwave and Optical Technology Letters. **55** (2013), 2186-2190.
15. R. TANABE and A.S. FUKUNAGA: *Improving the search performance of SHADE using linear population size reduction*. Proceedings of the IEEE Congress on Evolutionary Computation (CEC), Beijing, China (2014), 1658-1665, <https://doi.org/10.1109/CEC.2014.6900380>.
16. V. STANOVOV and E. SEMENKIN: *Surrogate-Assisted Automatic Parameter Adaptation Design for Differential Evolution*. Mathematics **2023** (year=2023), <https://api.semanticscholar.org/CorpusID:259620840>.
17. G. ARISTARKHOV and N. ZVEZDINOV: *High-Selectivity Single- and Dual-Resonator Microstrip Filters*. J. Commun. Technol. Electron. **62** (2017), 916-920.
18. R. STORN and K. PRICE: *Differential evolution – a simple and efficient heuristic for global optimization over continuous spaces*. Journal of Global Optimization, **11(4)** (1997), 341-359, <https://doi.org/10.1023/A:1008202821328>.
19. R. TANABE and A.S. FUKUNAGA: *Success-history based parameter adaptation for differential evolution*. Proceedings of the IEEE Congress on Evolutionary Computation (2013), 71-78, <https://doi.org/10.1109/CEC.2013.6557555>,
20. J. ZHANG and A. C. SANDERSON: *JADE: Self-adaptive differential evolution with fast and reliable convergence performance*. 2007 IEEE Congress on Evolutionary Computation, (2007), 2251-2258.
21. V. STANOVOV, S. AKHMEDOVA and E. SEMENKIN: *Selective Pressure Strategy in differential evolution: Exploitation improvement in solving global optimization problems*. Swarm Evol. Comput., **50** (2019).
22. V. STANOVOV, S. AKHMEDOVA and E. SEMENKIN: *LSHADE Algorithm with Rank-Based Selective Pressure Strategy for Solving CEC 2017 Benchmark Problems*. 2018 IEEE Congress on Evolutionary Computation (CEC), (2018), 1-8
23. V. STANOVOV and E. SEMENKIN: *Surrogate-Assisted Automatic Parameter Adaptation Design for Differential Evolution*. Mathematics. **11(13)** (2023), 2937, <https://www.mdpi.com/2227-7390/11/13/2937>. ISSN = 2227-7390, DOI = 10.3390/math11132937